RSC Advances

PAPER

View Article Online
View Journal | View Issue

Cite this: *RSC Adv.*, 2021, **11**, 34479

Curcumin-loaded metal oxide aerogels: supercritical drying and stability†

Wael Hamd,‡ Digambara Patra and Houssam El-Rassy *

Received 6th September 2021
Accepted 18th October 2021

DOI: 10.1039/d1ra06693e

rsc.li/rsc-advances

Curcumin, known as a potential antioxidant and anti-inflammatory agent, has major limitations for its therapeutic use because of its lack of water solubility and relatively low bioavailability. We report for the first time the loading of different metal oxide aerogels with curcumin. The aerogels were prepared *via* the sol–gel process and dried under supercritical conditions. Mixing curcumin with the metal precursors prior to the formation of the solid network ensures maximum entrapment. The curcumin–network interactions stabilize the organic moiety and create hybrid aerogels as potential vehicles for curcumin in various media. The aerogels were characterized by FTIR spectroscopy, thermogravimetric analysis, electron microscopy, and fluorescence spectroscopy to confirm their hybrid nature. The stability study by fluorescence spectroscopy revealed three distinct behaviors depending on the nature of the metal oxide: (i) a minor interaction between curcumin and the solid network slightly affecting the microenvironment; (ii) a quenching phenomenon when iron is present explained by a coordination between the iron ions and curcumin; and (iii) a strong complexation of the metal ions with curcumin after gelation.

1. Introduction

Metal oxide aerogels are highly porous materials with remarkably large surface areas.[1] These materials are prepared from different metal precursors according to the sol–gel technique,[2] either through the hydrolysis and condensation route,[3] by polymer crosslinking,[4] or *via* the epoxide-assisted approach.[5] The gel network starts with the hydrolysis of the metal precursors, in aqueous media or in organic solvents, thus leading to the formation of hydroxo ligands. These latter condense *via* deprotonation, olation, or oxolation processes making the seeds for a wider three-dimensional expansion of the network.[6] The formation of the gel is a complicated transition that depends on several critical parameters, including but not limited to, the concentration of the precursors, the order of mixing of the precursors, and the temperature.[7]

The formation of the alcogel is followed by a supercritical drying. Several metal oxide aerogels prepared according to this technique have been reported in the literature such as silica (SiO_2),[3] titania (TiO_2),[8] alumina (Al_2O_3),[9] zirconia (ZrO_2),[10] iron oxide (Fe_2O_3),[11] cobalt-ferrite ($CoFe_2O_4$),[12] neodymium oxide (Nd_2O_3),[13] dysprosia (Dy_2O_3),[14] holmia (Ho_2O_3),[13] erbia (Er_2O_3),[13] samaria (Sm_2O_3),[13] and vanadia (V_2O_5).[15]

To the interesting porosity of the aerogels are added their molecular homogeneity[16] and the possibility of their preparation in bulk. Although these materials were reported for the first time in 1931 by S. S. Kistler,[17] their broad range of technological applications increased noticeably in the last decades with potential uses for thermal[18] and acoustic insulation,[19] photoluminescence[20] and radioluminescence devices,[21] as adsorbents,[8,22–25] catalysts,[12,26] and catalyst supports.[27–30] Furthermore, hybrid organic–inorganic aerogels were found to be promising materials as optical components,[31,32] insulating materials in microelectronics,[33] host materials for sensors,[34] and for drug delivery.[35]

Curcumin (IUPAC name: (*E*)-1,7-bis(4-hydroxy-3-methoxyphenyl)hept-3-ene-1,6-dione) is a polyphenol extracted from the *Curcuma Longa* rhizomatous herbaceous perennial plant. This molecule was found to benefit several medical conditions[36–39] mainly due to its antioxidant and anti-inflammatory effects.[39,40] In addition to its medicinal applications, curcumin can be used for fluorescence probing[41,42] and sensing applications.[43,44] Several encapsulation and loading media were investigated to enhance the stability of curcumin and widen its spectrum of use. Liposomes,[45] emulsions,[46] nanoemulsions,[47] CD-MOFs,[48] biopolymeric microgels,[49] solid lipid nanoparticles,[50] polystyrene-based nanoparticles,[51] polymeric nanoparticles,[52] chitosan–folate mesoporous silica nanoparticles,[53] mesoporous silica nanoparticles,[54] porous discoidal polymeric particles,[55] nanoporous starch aerogels,[56] collagen aerogels,[57] and pectin aerogels[58] were found to improve the

Department of Chemistry, American University of Beirut, P. O. Box 11-0236, Riad El-Solh 1107 2020, Beirut, Lebanon. E-mail: Houssam.Rassy@aub.edu.lb; Tel: +961-1-374374 ext. 4051

† Electronic supplementary information (ESI) available. See DOI: 10.1039/d1ra06693e

‡ Current address: Department of Chemical Engineering, Faculty of Engineering, University of Balamand, P.O. Box 33 Amioun, El Koura, Lebanon.

stability of curcumin whenever it is encapsulated within their networks or loaded on their surfaces.

We report herein the use of metal oxide aerogels as encapsulation media for curcumin. A wide range of aerogels were considered where curcumin was mixed with the metal precursors pre-condensation. This work aims to achieve the best entrapment of the organic moiety within the inorganic network, and to explore the interactions existing between them. To do so, the curcumin–network interaction and the stability of the hybrid aerogels were studied under various conditions.

2. Materials and methods

2.1. Materials

The chemicals were used as received and without further purification. Tetraethoxysilane, titanium(IV) isopropoxide, dysprosium(III) chloride hexahydrate, holmium(III) chloride hexahydrate, neodymium(III) chloride hexahydrate, erbium(III) chloride hexahydrate, and samarium(III) chloride hexahydrate were purchased from Sigma-Aldrich. Cobalt(II) chloride hexahydrate was provided by AnalaR. Iron(III) chloride hexahydrate was from Fluka. Curcumin (98% purity) and propylene oxide were purchased from Acros Organics. Methanol, hydrochloric acid (37%), and ammonium hydroxide were from Riedel-de-Haen, Panreac and Fischer Scientific, respectively. Double deionized water was prepared in our laboratory.

2.2. Synthesis of hybrid aerogels

The inorganic–curcumin aerogels were prepared *via* a two-step sol–gel process using various metal precursors followed by carbon dioxide supercritical drying.

Dysprosium, holmium, neodymium, erbium, and samarium oxide aerogels were prepared as follows: 1.0 mmol of the metal salt was dissolved in 2.0 mL of methanol for 1 min to which 1.0 mL curcumin solution (10^{-3} M in methanol) was then added. The mixture was left under magnetic stirring for a few minutes, followed by rest at room temperature. The gelation of the sol was observed in the next 24 h and the obtained gels were kept for aging over one additional day at room temperature. The gels were soaked in acetone for 24 h to allow for the residual water and methanol to be exchanged with acetone presenting a higher miscibility with liquid carbon dioxide. The samples were then dried under supercritical carbon dioxide ($T_c = 31.1$ °C; $P_c = 73.7$ bar) leading to the final hybrid aerogels.

Silica, titania, and cobalt ferrite aerogels were prepared as per ref. 48, 10, and 14, respectively. Curcumin was added to the mixture prior to gelation with a molar ratio metal : curcumin equal to $1 : 10^{-3}$.

2.3. Characterization of hybrid aerogels

FTIR spectroscopy measurements were performed on a Thermo-Nicolet 4700 Fourier Transform Infrared Spectrometer equipped with a Class 1 laser using the KBr technique. The Thermogravimetric Analysis (TGA) was performed on a NETZSCH TG 209 F1 Libra with a heating rate of 5 °C min^{-1} between room temperature and 520 °C. The surface morphology of the aerogels was observed using scanning electron microscopy (SEM) performed on a MIRA3 Tescan electron microscope after coating the samples with a thin layer of gold. Fluorescence microscopy was performed on a Leica DM6 B upright fluorescence microscope equipped with a Leica DFC7000 T microscope camera. UV-visible spectroscopy measurements were conducted on a V-570 UV/VIS/NIR spectrophotometer from JASCO. Fluorescence spectroscopy was performed on a Fluorolog-3 spectrofluorometer from Jobin Yvon Horiba equipped with a MicroMax 384 microwell-plate reader and DataMax V2.2 acquisition and analysis software.

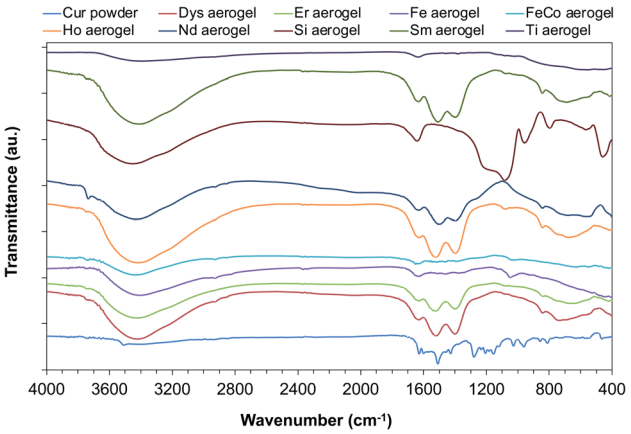

Fig. 1 FTIR spectra of hybrid aerogel samples.

3. Results and discussion

3.1. FTIR spectroscopy

The FTIR spectrum of the free curcumin (Fig. S1†) showed a sharp peak at 3510 cm^{-1} corresponding to the O–H stretching vibration of the phenolic group[59] with a broad band between 3500 and 3200 cm^{-1} attributed to the ν(OH) group in the enol form. The low intensity peaks observed in the 3000–2850 cm^{-1} range are assigned to the stretching vibrations of C–H bonds. The intense absorption band at 1629 cm^{-1} is attributed to the carbonyl group (C=O)[59] and the band at 1603 cm^{-1} corresponds to the symmetric aromatic ring stretching vibrations.[60]

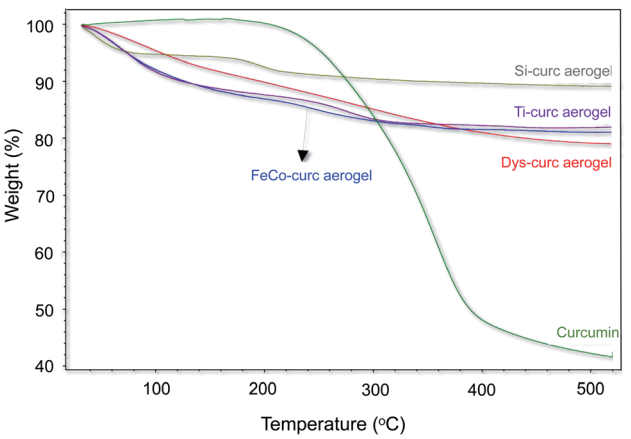

Fig. 2 TGA curves recorded for the free curcumin and for some hybrid aerogels.

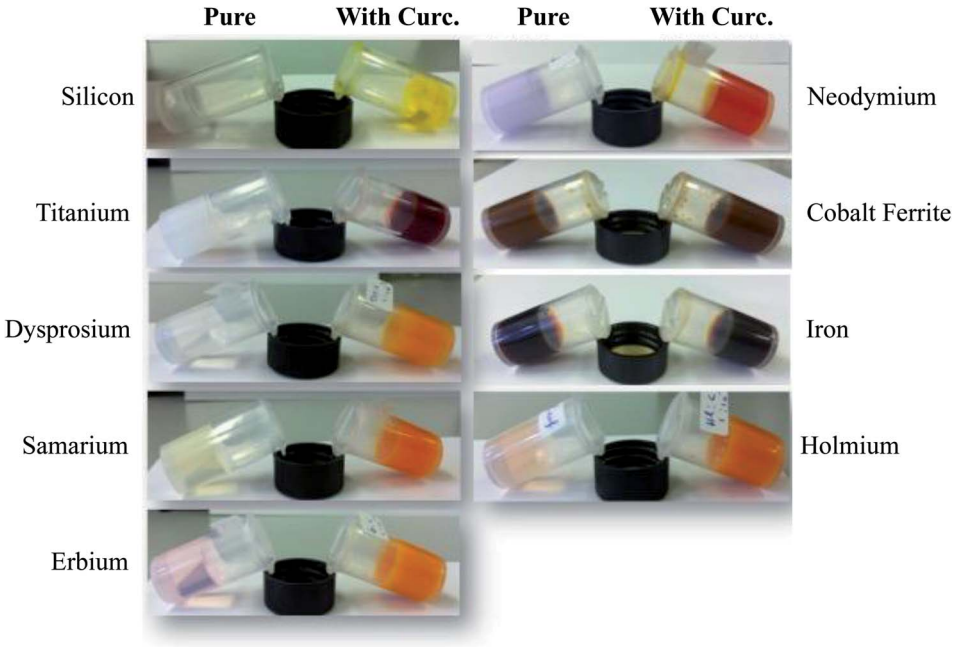

Fig. 3 Photos of wet alcogels with and without curcumin.

The intense peak at 1508 cm^{-1} is attributed to the mixed vibrations of ν(C=O), δ(CCC), δ(CC=O) and aromatic ν(CC), ν(CCH). The band at 1282 cm^{-1} is the overlapping of the in-plane C–H vibrations of aromatic rings and the C–O stretching.[59] The peaks appearing at 962 and 809 cm^{-1} are attributed to the C–H bending of alkene.[61]

The FTIR spectra of the aerogels after curcumin encapsulation revealed the presence of characteristic peaks of curcumin (Fig. 1). This confirms the entrapment of the organic molecule within the inorganic networks and the formation of a hybrid aerogel. The peaks appearing in the range 3000–2850 cm^{-1}, at 1629 cm^{-1} and 1508 cm^{-1} for the hybrid material are typical examples.

3.2. Thermogravimetric analysis

The presence of curcumin in the hybrid aerogels has been confirmed by TGA where the weight loss profiles for the free curcumin and for the hybrid aerogels have been compared (Fig. 2). A major weight loss (~58%) was observed for the free curcumin above 200 °C with no losses observed at lower temperatures. Similar weight losses were seen for the hybrid aerogels in addition to a weight loss at *ca.* 100 °C that corresponds to the loss of weakly bonded water molecules to the aerogels surface. These TGA curves confirm the retention of the curcumin molecules within the solid network even after soaking

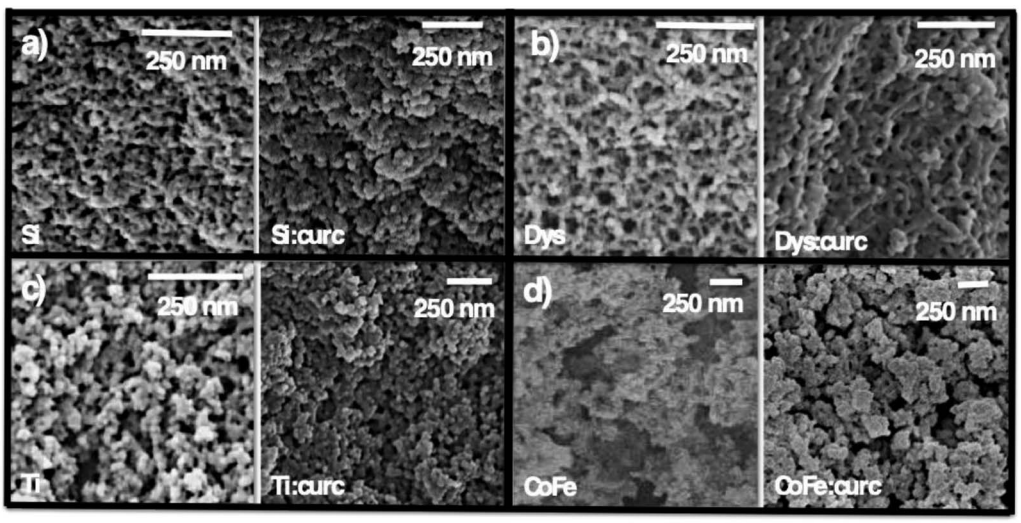

Fig. 4 SEM micrographs of some selected inorganic and hybrid aerogels. (a) Si and Si–Curc; (b) Dys and Dys–Curc; (c) Ti and Ti–Curc; (d) CoFe and CoFe–Curc.

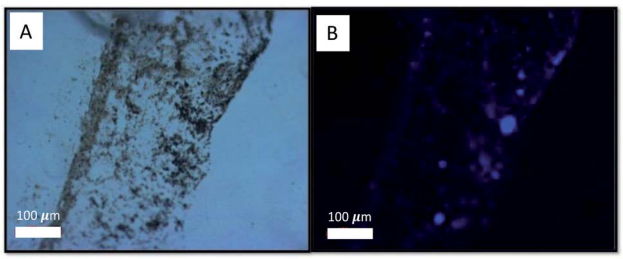

Fig. 5 Fluorescence microscopy images of silica–curcumin aerogel. (A) White light excitation, (B) excitation at 365 nm.

the gel pre-drying in acetone for 24 hours. The difference in the weight losses between the various studied aerogel media is an indicator of the disparity in curcumin binding with the various inorganic aerogels.

3.3. Imaging and electron microscopy

A macroscopic view of the inorganic and hybrid gels shows that some inorganic gels are transparent whereas some others are not. This is due to a difference in the kinetics of the hydrolysis and condensation of the precursors leading to a difference in the size of the secondary particles. Instead, all hybrid gels obtained after mixing the curcumin solution with the inorganic precursor sols are opaque (Fig. 3). The increase in the light scattering is due to the presence of curcumin molecules within the inorganic matrix thus affecting the pore network. Soaking the gels in acetone for 24 h followed by the drying process under supercritical conditions shows that the color of the curcumin-containing gels does not change. This suggests that the soaking and drying processes do not affect the presence of the curcumin moiety within the hybrid network.

The surface morphology of the aerogels observed by scanning electron microscopy unveils the amorphous nature of the material exhibiting large interconnected pores (Fig. 4). The comparison of the SEM micrographs for the inorganic and hybrid aerogels shows that the presence of curcumin within the inorganic matrix leads to a denser structure and reduces the porosity without completely suppressing the porous nature of the network. SEM micrographs for all hybrid aerogels are shown in Fig. S2.†

3.4. Fluorescence microscopy

The intrinsic fluorescence of curcumin was visualized using fluorescence microscopy. Conversely to the excitation using a white light that did not show any fluorescence, the excitation at 365 nm of the silica–curcumin aerogel showed a well-dispersed blue fluorescence withing the aerogel (Fig. 5). It is worth mentioning that a weak green fluorescence was seen when an excitation wavelength between 400–450 nm has been used (data not shown) and no fluorescence was observed outside this wavelength range. This confirms the presence and dispersion of the curcumin moiety within the hybrid matrix.

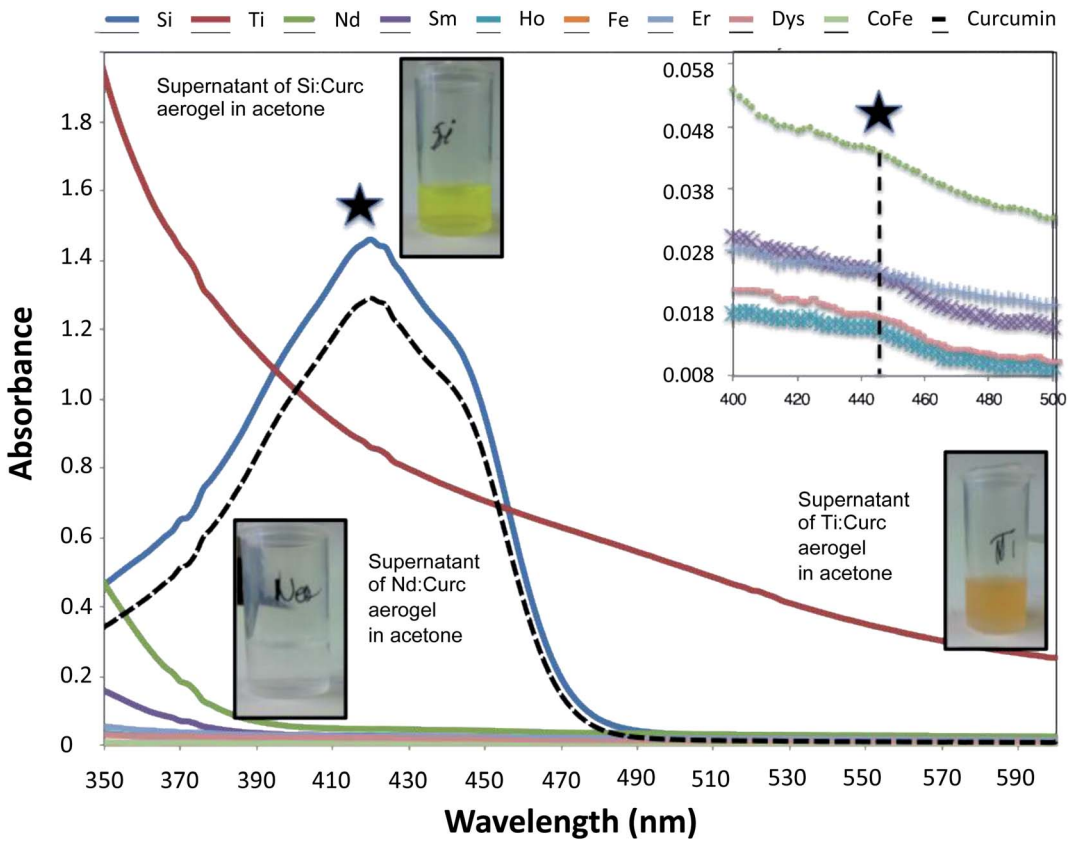

Fig. 6 UV-visible absorption spectra of supernatants obtained after dissolution of hybrid gels in acetone.

3.5. Curcumin release from hybrid alcogels in acetone

Since the wet gels were immersed in acetone for one day prior to the supercritical drying, the release of curcumin in acetone was studied using UV-visible spectroscopy. For that purpose, a calibration curve was performed at the maximum absorption wavelength 425 nm (Fig. S3†). The molar extinction coefficient (ε) found to be 40 000 M^{-1} cm^{-1} is in good agreement with the reported values in the literature.[62] To conduct the curcumin release experiments, 100 mg of each hybrid alcogel were suspended in 4 mL of acetone for one day under stirring, followed by a separation of the liquid phase.

The absorption spectrum of curcumin is recorded and compared to the spectra of the supernatants (Fig. 6). Curcumin in acetone showed a broad characteristic absorption band between 350 and 500 nm centered at 425 nm, with a shoulder around 460 nm. The maximum of this band is attributed to the electronic dipole allowed π–π* type excitation of its extended π-conjugation system.[63] An identical absorption band was observed for the silica–curcumin supernatant without any shift in wavelength. This suggests that a fraction of the curcumin is incorporated within the pores and does not undergo any chemical interaction with the silica network, and that the interaction between the curcumin moiety and the network is limited to some physical interactions. This conclusion is further supported by the yellow color of the supernatant identical to that of the free curcumin in acetone. The quantification by UV-visible spectrometry of released curcumin revealed that 35% of the initial amount diffused out of the network. Conversely, the color of the supernatant collected from the other curcumin-gels in acetone was not yellow. This suggests either a complexation between the curcumin molecules and the metal when a color is observed, a strong curcumin–network interaction and a complete retention of the organic molecule within the network when the acetone remained transparent, or a quenching phenomenon. In the case of titania–curcumin, the color of the supernatant is orange suggesting a complexation of the titanium with curcumin. The quantification was not possible since the supernatant contained small particles increasing the light scattering and making the analysis inaccurate. No absorption in the whole study range was observed for the iron oxide and cobalt–iron oxide gels suggesting a quenching phenomenon due to the presence of iron in the gels. For all other gels, the release of curcumin was very weak. It was confirmed by the color of the supernatant which was almost transparent (see neodymium supernatant as an example, Fig. 6) coupled with a very weak absorption peak observed (see inset) at 445 nm. The shift in the maximum absorption peak from 425 to 445 nm suggests the involvement of the carbonyl group of curcumin in the metal complexation. This explains the retention of curcumin within the inorganic networks and the very small quantity released in the acetone. The shoulders at 445 nm are probably due to a curcumin (L) → metal (M^{n+}) charge transfer[64] and the small shift in the absorption peak between the different complexes depends on the nature of the metal ion.

To assess the diffusion of curcumin from the solid networks, curcumin–silica gel was selected as a model. The hybrid gel was immersed in 100 mL of acetone and kept under stirring for 72 h. The quantification of curcumin present in aliquots taken at various time intervals shows a gradual increase in the concentration of curcumin in the medium and a plateau reached after 72 h. Plotting the concentration of released curcumin *versus* the square root of time (Fig. 7) shows a perfect linearity revealing that this release follows the Higuchi model[65] applicable to the release of drugs incorporated within the solid matrices. This model describes the release based on a Fickian diffusion equation as follows $R = K_H t^{1/2}$, where R is the amount of drug released, t is time, and K_H is the Higuchi dissolution constant.

3.6. Dissolution of hybrid aerogels in THF

After immersion in acetone for one day, the gels were dried under supercritical conditions leading to the aerogels. To confirm the retention of curcumin within the solid network of the hybrid aerogels, these latter were dissolved in THF and their UV-visible absorption spectra were compared to that of curcumin in the same solvent. Except silica and titania, all other aerogels showed quite a good solubility in THF thus allowing a qualitative assessment. Curcumin in THF showed, like when dissolved in acetone, a broad absorption band between 350 and 500 nm with a maximum absorption at 425 nm and a shoulder around 450 nm (Fig. 8). On the other hand, three bands were observed for the dissolved aerogels at 360 nm, 450 nm, and 490 nm. The presence of a new broad band at 360 nm and the

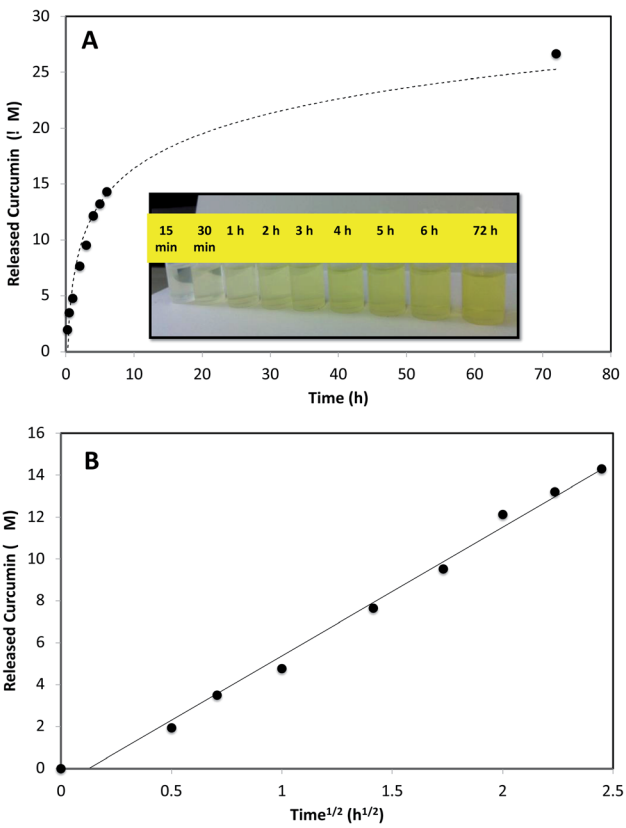

Fig. 7 (A) Release of curcumin from curcumin–silica hybrid gel in acetone; (B) concentration of released curcumin *vs.* time$^{1/2}$.

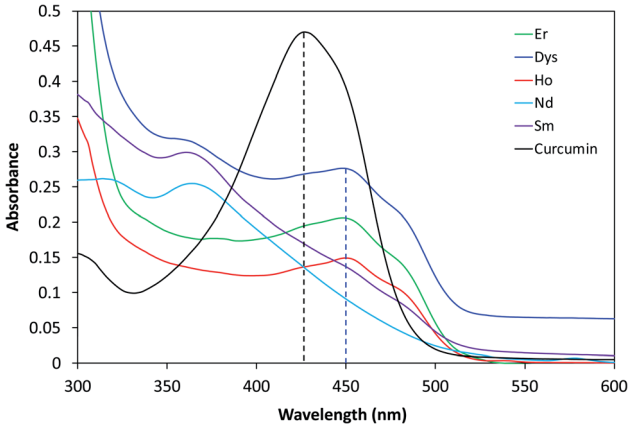

Fig. 8 UV-visible absorption spectra of hybrid aerogels after dissolution in THF.

shift of the characteristic peaks for curcumin indicate a change in the environment of curcumin. The shift of 25 nm observed for the π–π* transition band corresponds probably to a curcumin (L) → metal (M^{n+}) charge transfer as explained earlier.

3.7. Study of the curcumin–network interaction

In order to study the interaction between the curcumin moiety and the metal oxide network for the various aerogels, fluorescence spectroscopy was used as tool to reveal any changes in the curcumin microenvironment. The emission spectra were recorded between 450 and 700 nm following an excitation at 425 nm (Fig. 9). This was done for the mixture of precursors pre-gelation (liquid state) and for the final aerogels (solid state). It is worth noting that the ratio metal-to-curcumin was 1.0×10^3.

The comparison of the fluorescence spectra of the hybrid aerogels to that of curcumin powder (Fig. 9B) reveals a noticeable blueshift of the maximum band from 560 nm for the free curcumin to 525 nm for the entrapped curcumin within the aerogels, coupled with a significant increase in the intensity for some of the hybrid aerogels. This blueshift observed for the Si–, Sm–, Ho–, Dys–, Er–, and Nd–curcumin hybrid aerogels, indicates a change in the curcumin microenvironment upon encapsulation within the inorganic networks. This can be due to either the interaction between the curcumin functional groups and the hydrophobic regions of the gels, or to some condensation process between the OH groups of the hydrolyzed inorganic precursors and the phenolic or *o*-methoxy groups in curcumin. A different behavior was observed in the case of Ti–, Fe– and FeCo–curcumin aerogels. We noted a redshift in the fluorescence band for the Ti–curcumin aerogel coupled with a huge decrease in the intensity. The presence of iron in Fe– and FeCo–curcumin aerogels seems to cause a complete extinct of the fluorescence signal.

To understand this behavior and explain what happens to the curcumin moiety within the solid networks, the emission spectra were recorded for the curcumin-precursors in the liquid state pre-gelation. Fig. 9A shows that, similarly to the solid state, the fluorescence in solution exists for all samples except the ones containing iron (*i.e.* Fe and FeCo). The extinction of the fluorescence signal before gelation attests for the strong interaction between the iron ion and curcumin. The transfer of electron density from the highly electron rich conduction band of curcumin to the lower energy band of iron becomes important. This electron density transfer leads to the formation of an electrostatically stable curcumin–iron complex and the iron–curcumin chelate formation is the main reason for the quenched fluorescence. The high fluorescence intensity for the Ti–curcumin solution confirms the absence of any quenching phenomenon and suggests that the large extinction of the fluorescence signal in the solid state is probably due to a change in the curcumin structure following the adding of concentrated nitric acid into the solution. It is important to mention that this measurement was done for a mixture without any HNO_3, since the very fast gelation observed a few seconds after the addition of the acid makes it impossible to perform the fluorescence measurements for the solution.

3.8. Recovery of curcumin from hybrid aerogels

The interaction between curcumin moiety and metal precursors was found to be strong as concluded from the weak release of

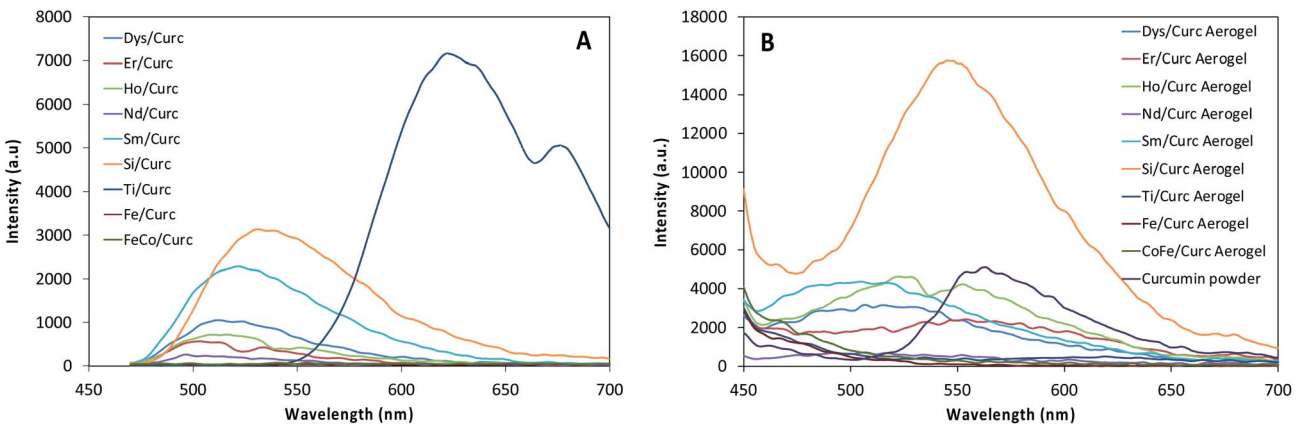

Fig. 9 Fluorescence spectra of (A) curcumin–inorganic precursors solutions before gelation; (B) curcumin–inorganic network after gelation at the solid state.

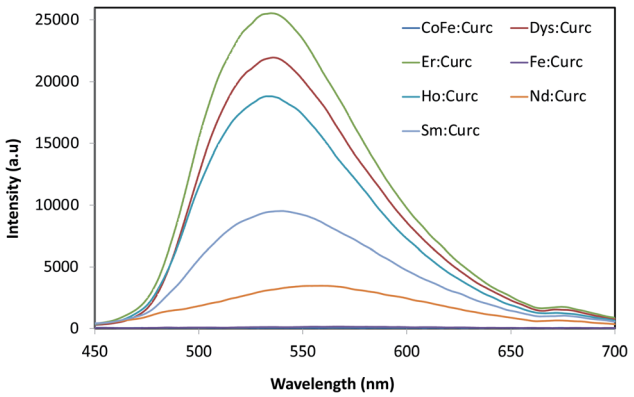

Fig. 10 Fluorescence spectra of dissolved hybrid aerogels in THF.

the encapsulated curcumin in acetone. In addition, we suppose that this interaction does not affect the structure of curcumin since the fluorescence experiments showed no major structural effect of the aerogel or its precursors except in the case of Ti–curcumin aerogel where nitric acid was used. To confirm this hypothesis, hybrid gels were dissolved in THF followed by fluorescence measurements. As mentioned earlier, the solubility of silica and titania in THF was very low and accordingly it was impossible to realize a propre fluorescence measurements for these samples. Fig. 10 shows that Er–, Dys–, Ho–, and Sm–curcumin hybrid aerogels exhibit a broad fluorescence band maximum at around 525 nm confirming the minor changes that take place during the gelation and after dissolution in THF (as compared to Fig. 9). On the other hand, the dissolved Nd–curcumin hybrid aerogel in THF revealed a band at around 550 nm similar to that of free curcumin. This suggests that the presence of this hybrid aerogel in THF weakens the interaction between the curcumin molecules and the solid network and allows the curcumin to freely exist in the solvent. Furthermore, the presence of iron in Fe– and FeCo–curcumin aerogels does not allow for any fluorescence to be observed, thus confirming the previous conclusion that the interaction between curcumin and iron-containing networks is very strong and consequently responsible for the quenching of any fluorescence signal.

4. Conclusion

Hybrid curcumin–metal oxide aerogels have been successfully prepared *via* the sol–gel process by loading of the aerogels with the organic moiety prior to the formation of the solid network. Dysprosium, holmium, neodymium, erbium, samarium, silicon, titanium, iron, and cobalt–iron oxides were explored in this study. The presence and dispersion of the curcumin moiety within the hybrid matrix were confirmed by various characterization techniques. The fluorescence spectroscopy revealed the strong curcumin–aerogel interaction and the high retention of the organic moiety within the hybrid network prior to the supercritical drying step. A different behavior was observed for the silica gel where 35% of the curcumin were found to diffuse out of the solid. Curcumin stability within the aerogel was also confirmed with a change in the curcumin microenvironment upon encapsulation within the inorganic networks. A shift of 25 nm observed for the π–π* transition band in UV-visible spectra corresponds probably to a curcumin (L) → metal (M^{n+}) charge transfer. The comparison of the fluorescence spectra of the hybrid aerogels to that of curcumin powder revealed either a blueshift or a redshift, depending on the nature of the metal oxide, also confirming changes in the microenvironment. The presence of iron in iron oxide and in cobalt iron oxide curcumin aerogels causes a complete extinct of the fluorescence signal.

Conflicts of interest

There are no conflicts of interest to declare.

Acknowledgements

The authors are thankful for the Kamal A. Shair Central Research Science Lab (KAS CRSL) of the Faculty of Arts and Sciences at AUB where the characterization was performed.

References

1 L. Manzocco, K. S. Mikkonen and C. A. García-González, *Food Struct.*, 2021, **28**, 100188.
2 C. J. Brinker and G. W. Scherer, in *Sol-Gel Science*, ed. C. J. Brinker and G. W. Scherer, Academic Press, San Diego, 1990, pp. xvi–18.
3 R. Al-Oweini and H. El-Rassy, *J. Mol. Struct.*, 2009, **919**, 140–145.
4 L. A. Capadona, M. A. B. Meador, A. Alunni, E. F. Fabrizio, P. Vassilaras and N. Leventis, *Polymer*, 2006, **47**, 5754–5761.
5 A. E. Gash, T. M. Tillotson, J. H. Satcher Jr, L. W. Hrubesh and R. L. Simpson, *J. Non-Cryst. Solids*, 2001, **285**, 22–28.
6 C. P. Alain, *Introduction to Sol-Gel Processing*, Springer Science + Business Media, New York, 1998.
7 J. Livage, M. Henry and C. Sanchez, *Prog. Solid State Chem.*, 1988, **18**, 259–341.
8 L. Abramian and H. El-Rassy, *Chem. Eng. J.*, 2009, **150**, 403–410.
9 A. C. Pierre, E. Elaloui and G. M. Pajonk, *Langmuir*, 1998, **14**, 66–73.
10 A. Lecomte, F. Blanchard, A. Dauger, M. C. Silva and R. Guinebretière, *J. Non-Cryst. Solids*, 1998, **225**, 120–124.
11 A. E. Gash, T. M. Tillotson, J. H. Satcher, J. F. Poco, L. W. Hrubesh and R. L. Simpson, *Chem. Mater.*, 2001, **13**, 999–1007.
12 J. Akl, T. Ghaddar, A. Ghanem and H. El-Rassy, *J. Mol. Catal. A: Chem.*, 2009, **312**, 18–22.
13 M. A. Worsley, J. Ilsemann, Th. M. Gesing, V. Zielasek, A. J. Nelson, R. A. S. Ferreira, L. D. Carlos, A. E. Gash and M. Bäumer, *J. Sol-Gel Sci. Technol.*, 2019, **89**, 176–188.
14 A. Bang, A. G. Sadekar, C. Buback, B. Curtin, S. Acar, D. Kolasinac, W. Yin, D. A. Rubenstein, H. Lu, N. Leventis and C. Sotiriou-Leventis, *ACS Appl. Mater. Interfaces*, 2014, **6**, 4891–4902.
15 V. Augustyn and B. Dunn, *C. R. Chim.*, 2010, **13**, 130–141.

16 J. B. Miller, S. E. Rankin and E. I. Ko, *J. Catal.*, 1994, **148**, 673–682.
17 S. S. Kistler, *Nature*, 1931, **127**, 741.
18 S. K. Adhikary, D. K. Ashish and Ž. Rudžionis, *Energy Build.*, 2021, **245**, 111058.
19 Z. Mazrouei-Sebdani, H. Begum, S. Schoenwald, K. v Horoshenkov and W. J. Malfait, *J. Non-Cryst. Solids*, 2021, **562**, 120770.
20 M. R. Ayers and A. J. Hunt, *J. Non-Cryst. Solids*, 1998, **225**, 343–347.
21 C. L. Renschler, J. T. Gill, R. J. Walko, C. S. Ashley, T. J. Shepodd, S. T. Reed, G. M. Malone, L. E. Leonard, R. E. Ellefson and R. L. Clough, *Radiat. Phys. Chem.*, 1994, **44**, 629–644.
22 N. Saad, M. Chaaban, D. Patra, A. Ghanem and H. El-Rassy, *Microporous Mesoporous Mater.*, 2020, **292**, 109759.
23 M. Chaaban and H. El-Rassy, *ACS Omega*, 2020, **5**(42), 27401–27412.
24 H. Ramadan, A. Ghanem and H. El-Rassy, *Chem. Eng. J.*, 2010, **159**, 107–115.
25 N. Saad, M. Al-Mawla, E. Moubarak, M. Al-Ghoul and H. El-Rassy, *RSC Adv.*, 2015, **5**, 6111–6122.
26 F. Kesserwan, M. N. Ahmad, M. Khalil and H. El-Rassy, *Chem. Eng. J.*, 2020, **385**, 123834.
27 H. El Rassy, A. Perrard and A. C. Pierre, *ChemBioChem*, 2003, **4**, 203–210.
28 H. El Rassy, A. Perrard and A. C. Pierre, *J. Mol. Catal. B: Enzym.*, 2004, **30**, 137–150.
29 C. Jalkh, C. Ghazaly and H. El-Rassy, *Mater. Chem. Phys.*, 2020, **252**, 123296.
30 R. Al-Oweini, S. Aghyarian and H. El-Rassy, *J. Sol-Gel Sci. Technol.*, 2012, **61**, 541–550.
31 B. Klemmed, L. v Besteiro, A. Benad, M. Georgi, Z. Wang, A. Govorov and A. Eychmüller, *Angew. Chem., Int. Ed.*, 2020, **59**, 1696–1702.
32 D. Shin, J. Kim, C. Kim, K. Bae, S. Baek, G. Kang, Y. Urzhumov, D. R. Smith and K. Kim, *Nat. Commun.*, 2017, **8**, 16090.
33 Y. Zhang, Q. Shen, X. Li, L. Wang and C. Nie, *Mater. Chem. Front.*, 2021, **5**, 4214–4224.
34 J. Yang, Y. Li, Y. Zheng, Y. Xu, Z. Zheng, X. Chen and W. Liu, *Small*, 2019, **15**, 1902826.
35 C. A. García-González, A. Sosnik, J. Kalmár, I. de Marco, C. Erkey, A. Concheiro and C. Alvarez-Lorenzo, *J. Controlled Release*, 2021, **332**, 40–63.
36 V. Kuptniratsaikul, P. Dajpratham, W. Taechaarpornkul, M. Buntragulpoontawee, P. Lukkanapichonchut, C. Chootip, J. Saengsuwan, K. Tantayakom and S. Laongpech, *Clin. Interventions Aging*, 2014, **9**, 451–458.
37 J. Trujillo, Y. I. Chirino, E. Molina-Jijón, A. C. Andérica-Romero, E. Tapia and J. Pedraza-Chaverrí, *Redox Biol.*, 2013, **1**, 448–456.
38 F. Mazzolani and S. Togni, *Clin. Ophthalmol.*, 2013, **7**, 939–945.
39 B. B. Aggarwal and K. B. Harikumar, *Int. J. Biochem. Cell Biol.*, 2009, **41**, 40–59.
40 S. C. Gupta, S. Patchva and B. B. Aggarwal, *AAPS J.*, 2013, **15**, 195–218.
41 D. Patra, E. el Khoury, D. Ahmadieh, S. Darwish and R. M. Tafech, *Photochem. Photobiol.*, 2012, **88**, 317–327.
42 E. D. el Khoury and D. Patra, *J. Phys. Chem. B*, 2013, **117**, 9699–9708.
43 M. Mouslmani, K. H. Bouhadir and D. Patra, *Biosens. Bioelectron.*, 2015, **68**, 181–188.
44 D. Patra, R. Aridi and K. Bouhadir, *Microchim. Acta*, 2013, **180**, 59–64.
45 M. Estephan, R. el Kurdi and D. Patra, *Colloids Surf., B*, 2021, **199**, 111546.
46 M. Kharat, G. Zhang and D. J. McClements, *Food Res. Int.*, 2018, **111**, 178–186.
47 H. Yu and Q. Huang, *J. Agric. Food Chem.*, 2012, **60**, 5373–5379.
48 Z. Moussa, M. Hmadeh, M. G. Abiad, O. H. Dib and D. Patra, *Food Chem.*, 2016, **212**, 485–494.
49 D. J. McClements, *Adv. Colloid Interface Sci.*, 2017, **240**, 31–59.
50 W. Wang, T. Chen, H. Xu, B. Ren, X. Cheng, R. Qi, H. Liu, Y. Wang, L. Yan, S. Chen, Q. Yang and C. Chen, *Molecules*, 2018, **23**, 1578.
51 M. Zatorska-Płachta, G. Łazarski, U. Maziarz, A. Foryś, B. Trzebicka, D. Wnuk, K. Chołuj, A. Karewicz, M. Michalik, D. Jamróz and M. Kepczynski, *ACS Omega*, 2021, **6**, 12168–12178.
52 A. Joseph, T. Wood, C.-C. Chen, K. Corry, J. M. Snyder, S. E. Juul, P. Parikh and E. Nance, *Nano Res.*, 2018, **11**, 5670–5688.
53 M. P. Daryasari, M. R. Akhgar, F. Mamashli, B. Bigdeli and M. Khoobi, *RSC Adv.*, 2016, **6**, 105578–105588.
54 D. Patra, D. Şen Karaman, D. Desai, E. el Khoury and J. M. Rosenholm, *Mater. Res. Bull.*, 2016, **84**, 267–272.
55 S. Aryal, S. Park, C. Park, M. J. Choi and J. Key, *Artif. Cells, Nanomed., Biotechnol.*, 2021, **49**, 390–396.
56 A. Ubeyitogullari and O. N. Ciftci, *Sci. Rep.*, 2019, **9**, 19112.
57 G. Dharunya, N. Duraipandy, R. Lakra, P. S. Korapatti, R. Jayavel and M. S. Kiran, *Biomed. Mater.*, 2016, **11**, 045011.
58 M. Pantić, G. Horvat, Ž. Knez and Z. Novak, *Molecules*, 2020, **25**(5), 1187.
59 S. Roy and J.-W. Rhim, *Int. J. Biol. Macromol.*, 2020, **162**, 1780–1789.
60 M. M. Yallapu, M. Jaggi and S. C. Chauhan, *Colloids Surf., B*, 2010, **79**, 113–125.
61 H. Kim, D. Kim, S. N. Karthick, K. V. Hemalatha, C. J. Raj, S. Ok and Y. Choe, *Int. J. Electrochem. Sci.*, 2013, **8**, 8320–8328.
62 A. Kunwar, A. Barik, R. Pandey and K. I. Priyadarsini, *Biochim. Biophys. Acta, Gen. Subj.*, 2006, **1760**, 1513–1520.
63 R. Waranyoupalin, S. Wongnawa, M. Wongnawa, C. Pakawatchai, P. Panichayupakaranant and P. Sherdshoopongse, *Cent. Eur. J. Chem.*, 2009, **7**, 388–394.
64 B. Zebib, Z. Mouloungui and V. Noirot, *Bioinorg. Chem. Appl.*, 2010, **2010**, 292760.
65 T. Higuchi, *J. Pharm. Sci.*, 1963, **52**, 1145–1149.